Hindawi
Structural Control and Health Monitoring
Volume 2024, Article ID 9687805, 19 pages
https://doi.org/10.1155/2024/9687805

Research Article

Fast Extraction Algorithm of Planar Targets Based on Point Cloud Data for Monitoring the Synchronization of Bridge Jacking Displacements

Dong Liang[1], **Zeyu Zhang**[1], **Qiang Zhang**[2], **Erpeng Wu**[3] and **Haibin Huang**[1]

[1]*School of Civil and Transportation Engineering, Hebei University of Technology, Tianjin, China*
[2]*Tianjin Highway Engineering Design and Research Institute Company Limited, Tianjin, China*
[3]*Tianjin Transportation Infrastructure Maintenance Group Company Limited, Tianjin, China*

Correspondence should be addressed to Zeyu Zhang; 202131603002@stu.hebut.edu.cn

Received 12 April 2023; Revised 19 January 2024; Accepted 30 January 2024; Published 13 February 2024

Academic Editor: Hoon Sohn

Transverse synchronization of vertical displacements of all jacking-up points is an important monitoring indicator to replace bearings in assembled multigirder bridges during the jacking phase. Currently, using target paper to identify the 3D coordinates of control points reduces the complexity of monitoring operations and improves the stability of data precision. However, the existing planar target locating methods have low accuracy, inefficiency, and subjectivity, which seriously hinders the construction process of bearing replacement. Accurately obtaining the center coordinates of multiple targets from a point cloud in a short monitoring period remains a challenge. This study proposes a high-precision automated algorithm to extract target center points in low-density point clouds to quickly calculate real target center points. First, we construct a standard point cloud model of the target papers for scanning, including color and geometric features. Then, we extract the measured point cloud of the typical jacking operation phase based on the reflection intensity and size information. Next, we map the intensity values of the measured point cloud into the color channel and register the measured point cloud with its standard point cloud model using the normal vector estimation and colored ICP algorithms. Finally, we extract the center point of the measured targets. Numerical experiments and engineering test results show that the proposed method converges quickly with high precision and good robustness, which saves 91.4% of the time compared with the traditional method. In general, this research can provide effective technical support for 3D laser scanning in monitoring the operation phase of bridge jacking.

1. Introduction

Against the backdrop of an aging infrastructure, the notable rise in traffic volume and load has resulted in cracking, severe compression deformation, and even disengagement of the rubber bearings in numerous bridges [1]. These bearing diseases severely restricted the free deformation of the structure, causing the structure to generate additional internal forces on the bearing capacity of the bridge [2]. The standard method of bearing replacement is to jack up the main girder, transfer the load from the bearing to a jack, subsequently replace the bearing, and ultimately transfer the load from the jack back to the bearing by dropping the girder [3]. The synchronization of the vertical displacement of each girder is an essential indicator in monitoring operations to prevent any potential harm to the main girder during construction [4].

The absolute vertical displacement at each jacking point on the main girder is an essential parameter for evaluating structural performance during construction. Currently, using linear variable displacement transducers is a prevalent approach for assessing the transverse relative displacement of bridge superstructures [5]. This method of displacement monitoring is basically possible since a fixed reference point can be used for installing the sensors. However, the conventional method of acquiring data from displacement sensors consumes many more monitoring instruments, and the time-consuming and laborious installation process also

interferes with the jacking operation. The limits of contact-type sensors make it very difficult to assess the safety of bridges. Therefore, an easy and fast method with stable data accuracy without causing girder damage is required. To address these problems, noncontact monitoring techniques have been developed.

The application of a 3D laser scanner presents a novel methodology for addressing the aforementioned challenges. LiDAR systems can acquire the overall shape of a structure with precise three-dimensional coordinates in a short period of time [6]. Therefore, the overall operational difficulty of main girder jacking displacement monitoring can be significantly reduced by extracting the centers of target papers pasted at each jacking point during different typical jacking operation phases. However, using the target extraction function in a terrestrial laser scanner requires the user to manually locate the approximate orientation of each target for rescanning. This procedure is not only ineffective, but it also introduces human subjectivity that compromises the stability of the extraction accuracy and cannot meet the demands of the bearing replacement project (Figure 1(a)). Thus, fast acquisition and accurate analysis of point cloud data constitute the core problem in 3D laser scanning monitoring of the synchronization of jacking displacement.

The displacement monitoring method of 3D laser scanning combined with target papers generally includes two steps: acquiring point cloud data and extracting target center coordinates. In point cloud data acquisition, a higher-density point cloud requires a longer scan time. Although high-density point clouds provide more detailed features that help obtain highly precise target center coordinates (Figures 1(b) and 1(c)), the longer scan time hampers the bearing replacement operation [7]. In target center coordinate extraction, the extraction of targets with structured features (sphere targets) is a research hotspot. For instance, Wu et al. [8] proposed a RANSAC point cloud spherical target detection and parameter estimation method based on principal curvature constraints. The method improves the fitting accuracy by constraining the quality of the sample points by the principal curvature. The extraction of targets has also utilized methods such as least squares (LSs) [9], feature-constrained grid search (FCGS) [10], 3D Hough transform [11], and cluster segmentation [12]. Nevertheless, installing these targets is a challenge, as maintaining their relative locations throughout the operation proves to be a difficult task. Using target papers effectively addresses this issue. There are relatively few studies on the extraction of unstructured features from point clouds for targets (planar targets) due to the fact that planar target point clouds do not have 3D features in 3D coordinates. The current approaches typically involve the transformation of 3D point clouds into 2D images, followed by applying well-established image processing techniques to extract unstructured features. However, this process is intricate, resulting in low extraction accuracy and underutilization of the high-precision 3D coordinates of the point clouds. Currently, the accuracy of target extraction algorithms relies on high-density point clouds, but this increases the monitoring time [13]. Thus, using low-density point cloud data to acquire high-precision target centers is the key to fast data extraction.

To address the above issues, an algorithm to achieve fast calculation of planar target center coordinates using 3D point cloud coordinates and intensity information is proposed based on synchronization monitoring of main girder jacking displacement in a bridge-bearing replacement project in Tianjin. To verify the accuracy of the algorithm, conventional displacement sensors were also installed in this construction project to monitor the vertical displacement of the main girder for comparison.

After the introduction section, the contents of the paper are organized as follows. Section 2 presents an overview of related work on displacement monitoring of structures using 3D laser scanning and point cloud extraction of target features. Section 3 describes the project background for this research. Section 4 describes the proposed algorithm for fast extraction of planar targets, which is accompanied by experimental tests. Section 5 describes the application of the proposed approach to an actual bearing replacement project. Finally, Section 6 concludes the study.

2. Related Work

2.1. Displacement Monitoring Method Using 3D Laser Scanning. In the field of structural health monitoring, the relative displacement of a structure is an important monitoring component as it provides direct information about the actual stiffness of the structure. 3D laser scanning can obtain geometric data with high speed and millimeter-level accuracy and has been extensively applied in structures' displacement and deformation monitoring. For instance, Farahani et al. [14] employed a camera and a circular laser module to construct a machine vision system for capturing a point cloud of the full 3D tunnel profile over time. The deformation variation undergone by the tunnel under compressive loading conditions could be identified by measuring the displacement field of the tunnel profile. Liang et al. [15] acquired two sets of spatial point cloud data for self-anchored suspension bridges with an interval of 2 years using 3D laser scanning. The changes in horizontal cable force and suspender force were obtained by comparing the displacements of the girders, cables, and tower tops. Cha et al. [16] proposed a novel method for monitoring the overall deflection of a structure based on point cloud data. The method continuously divided the point cloud space to create internal nodes, and the vertical displacement value was calculated by searching for the nodes where the deformation occurred. Yunmei et al. [17] proposed a multipoint chain laser detection method for dynamic deflection of super long-span bridges, which realizes real-time acquisition of multipoint displacements of bridges by constructing a multipoint deflection parameter detection model based on chain laser reference and image processing. Zvegintsev and Kislovsky [18] used 3D laser scanning to monitor the linear alignment of a rigid skeleton arch bridge during construction. They extracted the deformation results of the ring section on the arch ring and columns by employing a radial sliding window algorithm based on the fitted polynomial curvature. Li et al. [6] used 3D laser scanning to predict the alignment of concrete cable-stayed bridge assemblies. The

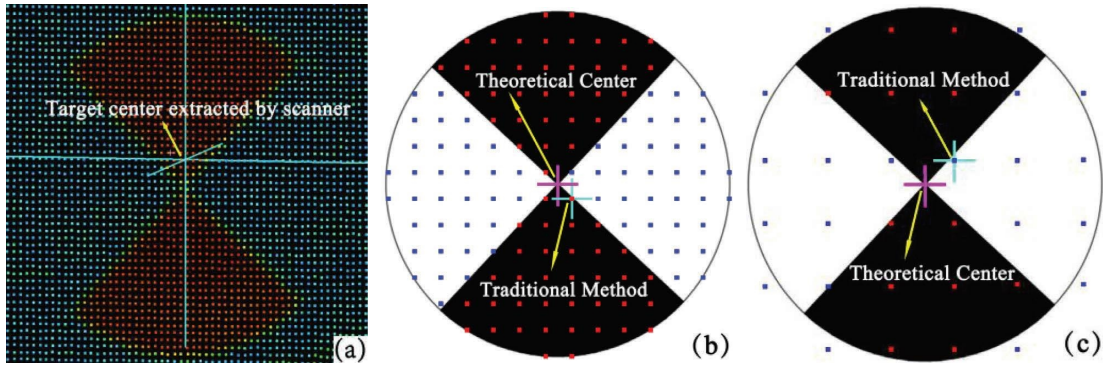

Figure 1: Extraction error of target center: (a) extraction error of scanner built-in algorithms, (b) extraction errors in high-density point clouds, and (c) extraction errors in low-density point clouds.

method utilizes target papers to identify the 3D coordinates of control points and virtual preassembly by aligning adjacent segment point cloud models to predict the bridge alignment. However, these methods are time-consuming in the data acquisition phase, which can lead to the inability to provide a timely solution for the deployment of adjustment operations during the jacking of the main girder, hindering the operational process of bearing replacement. In addition, these methods are neither accurate nor efficient when extracting the coordinates of the same feature points at different times under the discontinuous and low-density point cloud environment. The relative positions of the monitoring points in jacking displacement monitoring must be the same in various construction stages. Therefore, the optimum strategy in practical applications is to use targets for the purpose of extracting the precise coordinates of the jacking points.

2.2. Feature Point Extraction Technique Based on Point Cloud Data. It is necessary to implement a target-based approach to monitor the displacement of the jacking point effectively. The process of extracting the target's central point is closely associated with the feature point extraction method, which relies on point cloud data. This study categorizes the target into two distinct types of characteristics: structured features and unstructured features, based on the different methods employed for their extraction. Structured features refer to targets with three-dimensional shape characteristics within a three-dimensional space. These targets can take the form of spherical or prismatic shapes. This type of feature has a shape expression in the point cloud and can be detected according to the spatial coordinate characteristics of the target. The unstructured feature is that the target has only two-dimensional features in three-dimensional space, such as planar targets. This target type lacks discernible characteristics that can be extracted from the coordinate space. Thus, its extraction relies on attribute information, such as intensity or color, derived from the point cloud model.

In terms of structured feature extraction from point clouds, Shi et al. [19] proposed an iterative algorithm for the center extraction of spherical targets. The method utilizes the centroid of the point cloud and the estimated radius of the spherical target as constraints and uses a grid search to determine the optimal solution of the parameters. Li et al. [20] designed a surface-fitting model for a spherical target and utilized the robust least-squares method to get the model parameters from a point cloud containing noise. Stalowska et al. [21] used the coordinate and intensity information of point clouds to detect planar cracks by their curvature and intensity variations. Zhou et al. [22] extracted the point clouds of the edges of circular holes in the plane by clustering and radius nearest neighbor algorithm. Habib and Lin [23] used a seeded region growing algorithm to extract point, planar, and line features from point clouds based on the kd-tree data structure. Yoshizawa et al. [24] used principal curvature values combined with polynomial fitting to extract features in the triangular mesh.

For unstructured feature extraction, the German company Leica has built-in a planar target recognition function in the 3D laser scanner, which is capable of manually locating the rough target position, and consequently, high-resolution scanning is performed in the vicinity. When a target is scanned, the acquisition software automatically calculates its center by applying an algorithm for its measurement. However, the algorithms implemented in commercial software are unknown for the most part [25]. In addition, the subjectivity and efficiency of the method are insufficient in engineering. Brenner [26] applied the SIFT method to extract feature points from the intensity information of the point cloud and the geometric constraint to exclude false matches. Combining 2D images with 3D point cloud processing algorithms is the current method with high efficiency and accuracy. Liu et al. [27] converted point cloud data into images, segmented the target using a neural network model, and estimated the target center coordinates using the pixel near the center of the target image. Alshawabkeh [28] used color images and point clouds to automatically extract planar linear features. The point cloud data with unstructured features are first converted into a series of 2D images with added color information, and then, the linear edges in the images are extracted using the Canny operator and finally mapped back to the 3D point cloud.

Nevertheless, the primary drawback of these algorithms is that the processing results depend strongly on the quality and resolution of the point clouds. Currently, there are

relatively few studies on the direct extraction of unstructured features from point clouds. The existing methods generally convert 3D point clouds into 2D images and then use more mature image processing techniques to extract unstructured features. However, the operation process is complicated, the extraction accuracy is low, and the high-precision 3D coordinates of point clouds are not fully utilized. Thus, the research primarily focuses on obtaining precise planar target center coordinates during operations using low-resolution point clouds with reduced collection periods.

3. Project Background

A bridge in Tianjin is a prestressed concrete continuous girder bridge, with its span arrangement being 23.764 m + 3 × 21.6 m + 23.764 m, its bridge length 117 m, transection arrangement 1.0 m (facility belt) + 11.0 m (carriageway) + 0.5 m (crash barrier), and the full width 12.5 m. The superstructure is a prestressed concrete girder, the substructure cylinder pier, and the bearing plate rubber bearing.

After a long time of service, the deflection of the bridge's main girder and the nonuniform settlement of its foundation have caused disengaging, aging, and cracking of the bearings and an inability for free deformation (Figure 2(a)); therefore, the need to replace its bearings and girder synchronous jacking technology is used for bearing replacement [29–31]. The transverse synchronization of its vertical displacement is an important monitoring index to prevent the relative displacement difference of each main girder from exceeding the limit value. Yet, due to the narrow space at the bearing, the installation of the traditional displacement gauge is complicated, and data loss and distortion caused by the working interference frequently occur (Figure 2(b)).

4. Extraction Method of the Center Coordinates of the Plane Target

The overall thinking of the intelligent extraction and registration algorithm for target papers is as follows: ① extract targets fast in the whole point cloud model of a typical jacking construction process with intensity and the actual size of the target as constraints, ② create a standard point cloud model of the target paper with color and geometric feature information as the matching source point cloud, ③ estimate the normal vectors of each target plane in the point cloud, ④ use the target point cloud of the typical jacking construction phase as the target point cloud and the colored ICP algorithm [32] for matching, ⑤ determine the center of the physical target by extracting the coordinates of the theoretical target center in the source point cloud after matching, and ⑥ calculate the vertical displacement of each main girder jacking from the coordinate difference. The algorithm flow is shown in Figure 3.

4.1. Coarse Extraction of Target Point Cloud Based on Intensity Information. Only the part with a similar intensity to the target is retained for the whole point cloud measured in the typical jacking phase. The DBSCAN clustering algorithm [33] is used for classification, and the classes that do not meet the size threshold of the target paper are deleted by calculating the size of the bounding box of each class in the point cloud.

4.1.1. Point Cloud Filtering Based on Intensity. Intensity is an additional parameter obtained in laser scanning measurements. It describes the mathematical relationship between the laser-transmitted power (P_T) and the received power (P_R) [34, 35]. The mathematical expression is as follows:

$$P_R = \frac{\pi P_T \rho \cos\alpha}{4R^2}\eta_{\mathrm{Atm}}\eta_{\mathrm{Sys}}, \tag{1}$$

where P_T is the transmitted signal power and η_{Sys} is the system transmission coefficient in (1), both dependent on the specifications of the scanner and their values remain constant during the scanning process. η_{Atm} is the atmospheric transport factor, which can be identified as a constant under a constant environment [36]. The angle of incidence (α) and scanning range (R_s) have negligible effects on the intensity magnitude at small scanning distances (within 15 m) [37, 38]. The most important influence on the intensity is the reflectance of the measured object (ρ), whose value is related to the physicochemical properties of the object surface [39]. Research shows that the color of the object's surface has the greatest effect on the laser signal power, followed by roughness [40].

Planar targets generally consist of geometric shapes with a significant difference in color (Figure 4). However, the color information cannot be directly obtained from the laser signal. It is then necessary to take photos of the scene within the scan area in batches and map the color information into the point cloud after the scanning. This process is time-consuming and can hinder construction progress [41, 42]. The color information has the greatest effect on the reflected intensity of the laser signal in an unchanging environment [43]. Pure black and white in the point cloud have more extreme reflection intensity values. Paper has less roughness than concrete surfaces, which contributes to target extraction in complex environments. Thus, intensity information can be used to extract planar targets. The laser signal provides the reflected intensity values, which are quickly obtained at the end of the first scan.

According to the given point cloud model $P = \{p_i\}, p_i \in R^4, i \in \{1, \cdots, N\}$, a description of the steps is given as follows: step 1: set *datamax* and *datamin*, the upper and lower limits for the extraction intensity; step 2: choose an arbitrary point $p \in P$ as the starting point, and traverse all points. If point p is within the intensity extraction threshold, it is then marked as a local point and put into C. If point p is not within the threshold, then $p \in Z, P = P - \{p\}$; step 3: repeat step 2 until $P = \varnothing$; step 4: outlier rejection is performed on the obtained point set C. Select a point $p \in C$, build a sphere with point p as the center of the circle, set the parameters *nb_points* as the minimum number of points in the sphere, and R_i is the radius of the sphere for calculating the number of points in the neighborhood of the point p. If the number of points in the sphere where point p is located is

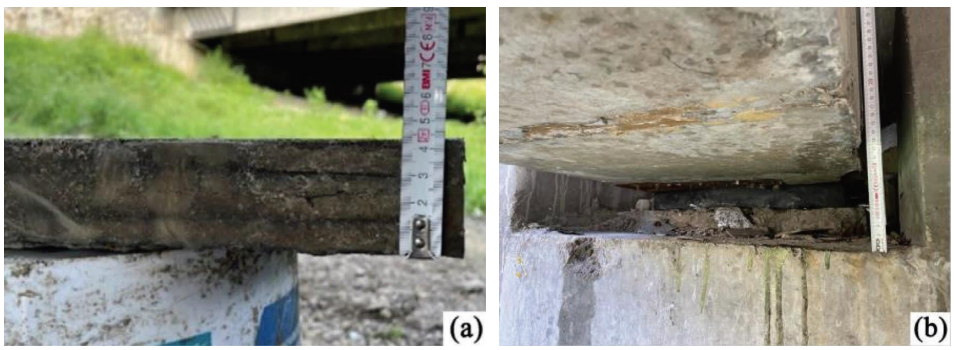

Figure 2: Bearing damage: (a) bearing aging cracking and unable to free deformation and (b) space for bearing work.

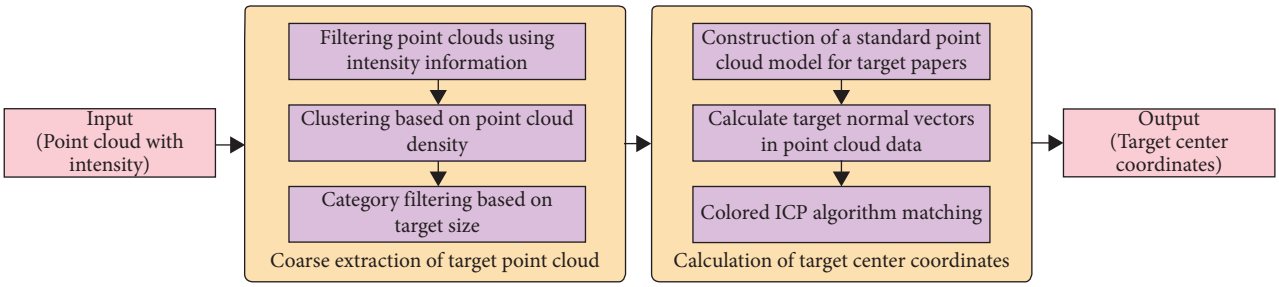

Figure 3: Fast extraction process of target center coordinates.

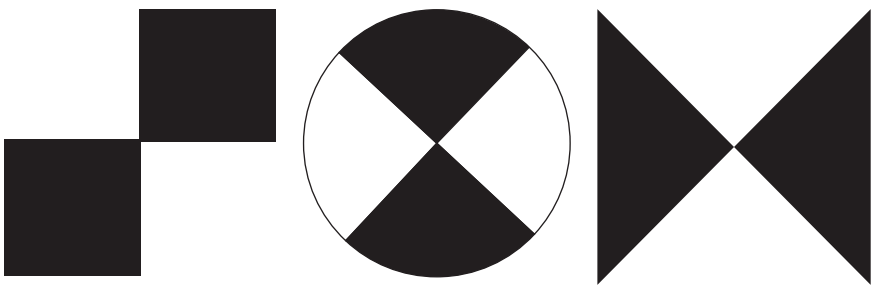

Figure 4: Various types of planar targets.

greater than *nb_points*, then point p is retained as a local point. If the number of points in the sphere where point p is located is less than *nb_points*, then point p is marked as an outlier, $p \in N, C = C - \{p\}$; step 5: repeat step 4 to instruct all data points to be marked, and the data point filtering is finished.

4.1.2. Clustering Based on Point Cloud Density. The intensity values of target papers are greatly different from their surroundings because of their pure black and pure white colors. After filtering according to the intensity, the remaining point clouds are not uniformly distributed and scattered in the environment. The point clouds at the targets are complete and homogeneous, so the density clustering algorithm can extract the point clouds containing the target.

In this paper, the DBSCAN clustering algorithm [33] is adopted as a tool for the initial extraction of the targets. The specific steps of the algorithm are as follows: step 1: draw a circle with eps as the radius, taking each data point x_i as the center of the circle. This circle is called the eps neighborhood of x_i. Step 2: examine the neighborhood formed by each point with eps as the radius. If the number of points in a particular neighborhood is above the set threshold *min_points*, then the center of that neighborhood is the core object. Any point that is not the core object but is still within the neighborhood of the core point is called a boundary point. A point that is neither a core point nor a boundary point is called a noise point. Step 3: repeat the above steps for all data points. The algorithm determines all data points to be either noise points, core points, or boundary points

(Figure 5), eliminates the noise points directly, and classifies into the same category the subcore points and their boundary points belonging to the same core point.

4.1.3. Coarse Extraction of Planar Targets. After the point cloud clustering, the classes that do not belong to the target need to be removed. The target paper has a fixed size. Therefore, by calculating the size of each class and comparing it with the actual size of the target, the classes that do not meet the size requirements can be removed, and finally, all the targets contained in the point cloud data can be extracted. However, the point cloud data are irregular and disordered, and the size information of the point cloud can be better illustrated by solving the optimal surrounding space of the 3D discrete data point set and estimating its size [44, 45]. The optimal surrounding space is usually a geometry with a simple shape. It is called a bounding box. Currently, the common ways to construct data point set bounding boxes are axis-aligned bounding box, bounding sphere, and oriented bounding box [46].

To estimate the size of each type of point cloud, the bounding box size needs to be calculated in order to completely and clearly extract the point clouds that meet the dimensions of the target. The target paper has a regular geometric shape in the point cloud. Hence, the axis-aligned bounding box is chosen to solve the dimensions for each type of point cloud, as shown in Figure 6.

4.2. Target Center Coordinates Extraction Method Based on Colored ICP Model Matching. The geometric and color features of target papers are fixed, so matching the standard point cloud model containing the theoretical target centers finely with the measured targets can improve the extraction accuracy and the iterative convergence of the algorithm. First, a high-density source point cloud model with geometric and color features of target papers is built. Then, the normal vector of each target in the target point cloud is calculated to achieve more accurate registration. Finally, the fine matching of the two point clouds is performed by the colored ICP algorithm. By extracting the center coordinates of the target from the source point cloud, the absolute coordinates of the target center are obtained.

4.2.1. Building a Standard Point Cloud Model of the Target Paper. The target paper's standard point cloud model is expressed by building a multidimensional matrix based on the Numpy programming library [47]. The point cloud is modeled according to the target paper's size, geometry, and color. The modeling steps are as follows:

Step 1: define the range datasize for the generation of the point cloud model (including the length, width, and height of the model)

Step 2: define the density ρ_s of the point cloud model, which in turn automatically calculates and specifies the position of each coordinate point in the point cloud model

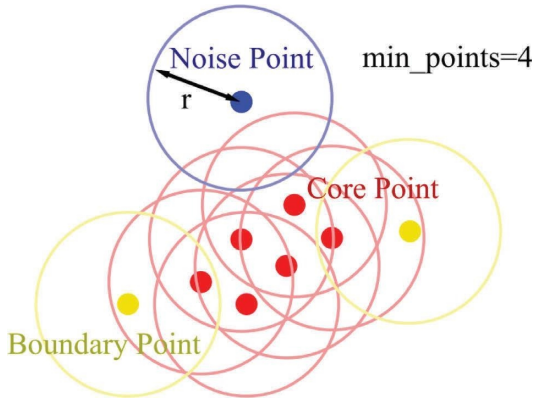

Figure 5: DBSCAN clustering schematic.

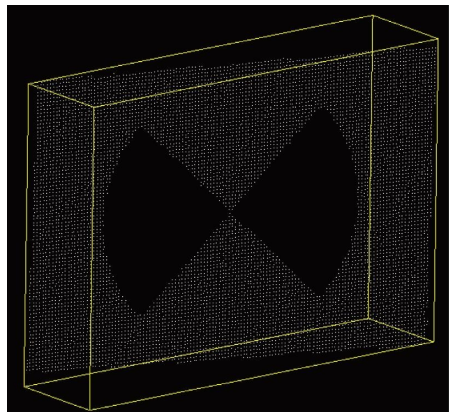

Figure 6: Axis-aligned bounding box.

Step 3: assign 3D coordinate (xyz) and color (rgb) information to each point, which in turn generates an empty matrix with six dimensions

Step 4: update the origin position and coordinate system, using the data point at the center of the target as the origin

Step 5: calculate the coordinate information and determine the color information one by one by cycling through the ranks of the matrix

(1) Coordinate information: Automatically calculated by the set datasize and ρ_s parameters.
(2) Color information: Judgment is made according to the constraints set by users. Take Figure 7 target paper as an example. When the circle equation satisfies $x^2 + z^2 > R$, the data points are marked as white; when the circle equation satisfies $x^2 + z^2 \leq R$ and $\pi/4 < \theta_s < 3\pi/4$ or $5\pi/4 < \theta_s < 7\pi/4$, the data points are marked as black. The rest of the data points are marked as white.

Step 6: repeat step 5 until all data points are judged, and the data are updated into the matrix

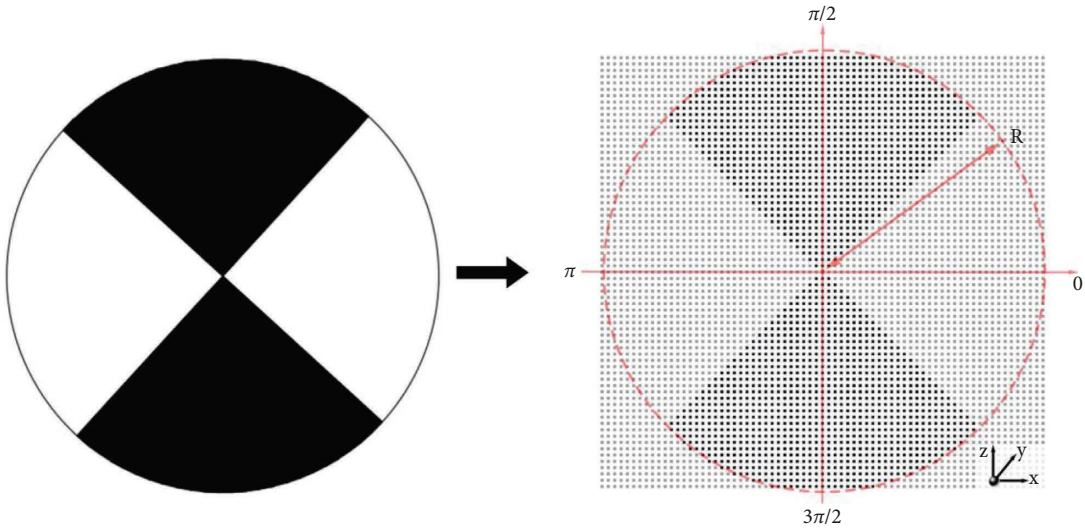

Target paper

Standard point cloud model of target paper

FIGURE 7: Diagram of the process of building the standard point cloud model of the target.

4.2.2. Estimation of the Normal Vector of the Target Plane. The use of point cloud normal can provide a better initial position for the matching point cloud and improve the accuracy and efficiency of the registration [48–50]. In this paper, the kd-tree algorithm is used to achieve fast retrieval of the nearest neighbors [51, 52]. When a set of neighborhood points is found and denoted $x_i \in R^n, i = 1, 2, \cdots, m$, a plane can be found in space (Figure 8(a)) such that a point c on this plane and its normal vector n satisfy:

$$\min_{c,n,\|n\|=1} \sum_{i=1}^{m} \left((x_i - c)^T n \right)^2, \tag{2}$$

where c is the centroid of x_i points, which can be expressed as $\bar{x} = 1/m \sum_{i=1}^{m} x_i$; the vector inner product is the projection of the neighboring points x_i on the normal vector n of the plane after subtracting the centroid c. In reality, it is impossible for all neighboring points to be exactly on the same plane. Therefore, the minimum value of their projection sum is used (Figure 8(b)).

Normalizing all data points, we get $\widetilde{X} = [\widetilde{x}_1, \cdots, \widetilde{x}_m], \widetilde{x}_i = x_i - \bar{x}, i = 1, \cdots, m$, and the problem is transformed into solving:

$$\min_{n \in R^n} \sum_{i=1}^{m} \left(\widetilde{x}_i^T n \right)^2, \text{s.t.} : \|n\|_2 = 1. \tag{3}$$

Expanding and recombining them gives

$$\min_{n \in R^n} n^T \widetilde{X} \widetilde{X}^T n, \text{s.t.} : \|n\|_2 = 1. \tag{4}$$

Equation (4) can be solved by using principal component analysis (PCA), using the eigenvector corresponding to the smallest eigenvalue in the solution $\widetilde{X}\widetilde{X}^T$ as the principal component. According to the definition of Rayleigh quotient $\lambda_{\min} x^T x \le x^T A x \le \lambda_{\max} x^T x$, the minimum eigenvalue of matrix A can be obtained [53]. Using the SVD decomposition for $\widetilde{X}\widetilde{X}^T$, we obtain $\widetilde{X}\widetilde{X}^T = U_r \Sigma^2 U_r^T$, and thus, the eigenvector corresponding to the smallest eigenvalue can be obtained from U_r.

4.2.3. Fine Matching of Target Point Clouds Based on Colored ICP. Color-based iterative closest point algorithm (colored ICP) [32] can jointly optimize geometric and color information and use the point-to-plane distance to calculate the geometric distance in the loss function $E(R, t)$. The geometric information is the distance between the tangent plane of the data points in the source point cloud and the corresponding points in the target point cloud. The color information is the difference between the color of the data points in the source point cloud and the projected color on the tangent plane of the corresponding points in the target point cloud. The loss function consists of two terms with empirically determined weights and is optimized iteratively during the registration period.

The point set $P = \left\{ p_1, \cdots, p_{N_p} \right\}, p_i \in R^6$ is given as the source point cloud, and the point set $Q = \left\{ q_1, \cdots, q_{N_q} \right\}, q_i \in R^6$ is given as the target point cloud, where P and Q are the point clouds of two colors. In order to take the color luminosity into account in the optimization function, a joint optimization function is, therefore, formulated, which is expressed as follows:

$$E(R, t) = (1 - \sigma) E_C(R, t) + \sigma E_G(R, t), \tag{5}$$

where E_C is the loss function of color luminosity, E_G is the loss function of geometric information, and $\sigma \in [0, 1]$ is set empirically to balance the weights of these two items. The two terms in (5) are solved, respectively, in the following section.

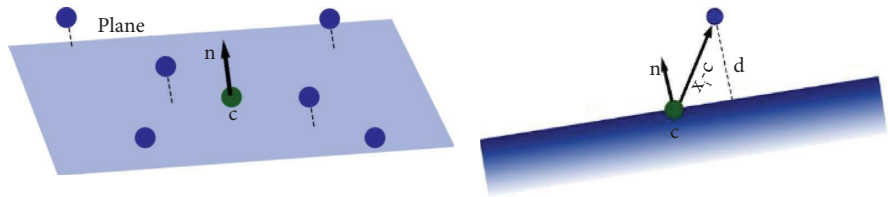

(a) (b)

Figure 8: Point cloud plane normal vector diagram.

(1) Solving for Color Information Items. Given that P is a set of points with color information, let $C(p)$ be a discrete function that can retrieve the color value of each point p_i. In order to be able to use the color luminosity information in the subsequent least-squares optimization function, it is necessary to reduce $C(p)$ to a continuous function so that its gradient can be calculated. To reduce it to a continuous function, a virtual orthogonal camera is conceptually introduced for each point $p \in P$, which observes the point along the direction n_p normal to the tangent plane of point p. The image observed by its virtual camera can be parameterized so that the color information of point p can be expressed as a continuous color function $C_p(u)$, where u is a vector emanating from point p along the tangent plane of point p, satisfying $u \cdot n_p = 0$. The function $C_p(u)$ can be expressed approximately as a first-order approximate expansion of this function at point p as follows:

$$C_p(u) \approx C(p) + d_p{}^T u, \tag{6}$$

where d_p is the gradient of the function $C_p(u)$, which can be calculated by applying least squares to the gradient of $\{C(p') \mid p' \in N_p\}$, where N_p is the point of the neighborhood of point p. To calculate the gradient, introduce the function $f(s)$, which is the function that projects the point s to the tangent plane of the point p and which satisfies

$$f(s) = s - n_p(s-p)^T n_p. \tag{7}$$

Thus, the least-squares optimization function for computing the gradient d_p changes to

$$L(d_p) = \sum_{p' \in N_p} \left(C_p(f(p') - p) - C(p')\right)^2 \approx \sum_{p' \in N_p} \left(C(p) + d_p{}^T (f(p') - p) - C(p')\right)^2. \tag{8}$$

Equation (8) satisfies the condition $d_p{}^T n_p = 0$. This allows solving the solution of this linear least-squares optimization, which in turn leads to the solution of the function C_p. Thus, the loss function $E_C(R,t)$ of the color luminosity part of the joint optimization function $E(R,t)$ can be defined as follows:

$$E_C(R,t) = \sum_{i=1}^{N} \left(C_p(q') - C(q)\right)^2. \tag{9}$$

The $q' = f(R,t)$ in (9), which is the projection function that satisfies (7).

(2) Solving for Geometric Information Items. The following section optimizes the loss function of geometric information in the joint optimization function $E(R,t)$. The traditional ICP registration method calculates the optimized value by point-to-point correspondence (pink dashed line in Figure 9); i.e., the data points in the source point cloud can only correspond to the data points that exist in the target point cloud. The error matrix is continuously iteratively calculated by calculating the corresponding point-to-point distances to minimize the error matrix. However, this distance calculation method is mostly wrong. Therefore, a simplified point-to-plane correspondence method is proposed to ensure computational speed and accuracy. This correspondence method can achieve more accurate matching by finding the corresponding point in the target point cloud and the plane formed by its neighbors and then calculating the distance from the point to the plane as the basis for the distance calculation. The point-to-plane distance calculation is shown in Figure 9.

Given the point set $P = \left\{p_1, \cdots, p_{N_p}\right\}, p_i \in R^3$ as the source point cloud, the point set $Q = \left\{q_1, \cdots, q_{N_q}\right\}, q_i \in R^3$ as the target point cloud, and n_i as the normal vector of the tangent plane at q_i; the error matrix can be defined as follows:

$$E(R,t) = \sum_{i=1}^{N} \left(\left(\mathrm{R}p_i + t - q_i\right)^T n_i \right)^2. \tag{10}$$

Conversion of the least-squares optimization function in (10), which can be solved linearly, will greatly simplify the solution of the problem. Since the iterative closest point (ICP) is an iterative algorithm, it can be assumed that the rotations and translations performed in each iteration will not be large, i.e., the rotation angles $\alpha, \beta, \gamma \longrightarrow 0$. Therefore, when $\theta \approx 0$, $\cos\theta \approx 1$, $\sin\theta \approx 0, \theta^2 \approx 0$. Thus, the rotation matrix R is as follows:

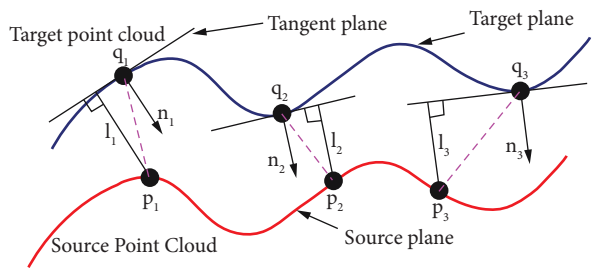

FIGURE 9: Calculation of point-to-plane distances in the iterative nearest point algorithm.

$$R \approx \begin{bmatrix} 1 & \alpha\beta - \gamma & \alpha\gamma + \beta \\ \gamma & \alpha\beta\delta + 1 & \beta\gamma - \alpha \\ -\beta & \alpha & 1 \end{bmatrix} \approx \begin{bmatrix} 1 & -\gamma & \beta \\ \gamma & 1 & -\alpha \\ -\beta & \alpha & 1 \end{bmatrix}. \quad (11)$$

Now, the loss function $E(R,t)$ contains 6 unknowns: $\alpha, \beta, \gamma, t_x, t_y, t_z$, which can be expressed in linear form and to which the flush coordinate transformation is applied:

$$E(R,t) = \sum_{i=1}^{N} \left(\left(\begin{bmatrix} R & t \\ 0 & 1 \end{bmatrix} \begin{bmatrix} p_i \\ 1 \end{bmatrix} - \begin{bmatrix} q_i \\ 1 \end{bmatrix} \right)^T \begin{bmatrix} n_i \\ 0 \end{bmatrix} \right)^2. \quad (12)$$

The solution of this function is obtained by organizing the loss function $E(R,t)$ into the form $Ax = b$, where $x = [\alpha, \beta, \gamma, t_x, t_y, t_z]^T$:

$$\hat{x} = \left(A^T A\right)^{-1} A^T b, \quad (13)$$

where $A = \begin{bmatrix} a_{11} & \cdots & a_{1z} \\ \vdots & \ddots & \vdots \\ a_{N1} & \cdots & a_{Nz} \end{bmatrix}$, $a_{i1} = n_{ix}p_{iy} - n_{iy}p_{iz}$, $a_{i2} = n_{ix}p_{iz} - n_{iz}p_{ix}$, and $a_{i3} = n_{iy}p_{iz} - n_{ix}p_{iy}$; $b = \begin{bmatrix} n_{1x}q_{1x} + n_{1y}q_{1y} + n_{1z}q_{1z} - n_{1x}p_{1x} - n_{1y}p_{1y} - n_{1z}p_{1z} \\ \vdots \\ n_{Nx}q_{Nx} + n_{Ny}q_{Ny} + n_{Nz}q_{Nz} - n_{Nx}p_{Nx} - n_{Ny}p_{Ny} - n_{Nz}p_{Nz} \end{bmatrix}$ in (13).

The rotation matrix R and translation matrix t are obtained by solving $\hat{x} = (A^T A)^{-1} A^T b$.

The algorithm fully uses 3D coordinates and reflection intensity information to extract planar targets automatically in a point cloud environment. By matching it with the standard point cloud model created by the Colored ICP algorithm, the center coordinates of the targets are extracted with high accuracy in the low-density point cloud.

4.3. Experimental Verification. Since multiple feature points need to be extracted during the jacking of the main girder, the proposed algorithm was used to perform the coordinate extraction of numerous target points, and the accuracy and reliability of the method were verified. In particular, the accuracy stability and algorithm convergence of the proposed method are verified by comparing the accuracy of target center extraction under different scanning resolutions. The accuracy of the proposed method is compared with that of the traditional method, and it is verified that the algorithm of this paper significantly improves the accuracy of target center extraction at lower scanning resolution.

4.3.1. Experimental Background. To verify the feasibility and accuracy of the above method, a Leica ScanStation P40 terrestrial 3D laser scanner and a total station were adopted to place six target papers with a radius of 0.1 m on the outdoor site. The configuration of the validation test is shown in Figure 10. To maximize the simulation of the actual scanning environment, the horizontal scanning distance was 15 m and the vertical angle was 30°. In this paper, four resolutions are selected for the experiment, namely, 12.5 m@10 m, 6.3 mm@10 m, 3.1 mm@10 m, and 1.6 mm@10 m, where 12.5 m@10 m means that the horizontal and vertical distance between neighbors in the point cloud is 12.5 m when the scanning distance is 10 m. The center coordinates of the targets are extracted by a 3D laser scanner and a high-precision total station. The coordinates collected by the total station are used as the theoretical values.

4.3.2. Analysis of Experimental Results. The experiment uses the data obtained from the total station as the theoretical coordinate value of the target center. Since the target paper is pasted on the wall, the calculated deviation value of the coordinates is mainly affected by the difference of the x and z directions. The influence of the y direction, which is perpendicular to the wall, is minimal. So, the extraction error is calculated by the following equation:

$$\Delta d = \sqrt{\Delta x^2 + \Delta y^2 + \Delta z^2}, \Delta y = 0, \quad (14)$$

where Δd represents the mutual difference between the theoretical coordinate value of the target center and the matched value, and Δx and Δz are the coordinate difference values in the corresponding directions.

This paper uses the k-nearest neighbor algorithm [54] to simulate the traditional target center extraction method. The theoretical target center coordinates are used as the sampling point, and the Euclidean distance between the sampling point and other points is calculated, from which the closest point to the sampling point is found as the result of the traditional extraction of the target center.

The scanning point clouds of the target papers at the four resolutions in the validation experiment are depicted in Figure 11. The scanner captures an initial number of 52,321,666 point clouds at the highest scanning resolution. The suggested technique successfully filtered the point clouds based on intensities and removed outliers, resulting in a remaining count of 116,895. This indicates that the proposed approach exhibits a significant efficiency level in filtering data during the coarse extraction phase. From Figure 12, it can be seen that the accuracy of the target center coordinates extracted with the algorithm in this paper is close to the accuracy measured by the total station and is much higher than that extracted with the traditional method. With the increase in scanning resolution, the density of the point cloud increases significantly. Although the extraction accuracy of the traditional method is improved, the error fluctuation is large and irregular. Thus, it cannot meet the engineering accuracy requirements. On the other hand, the proposed algorithm can still maintain the

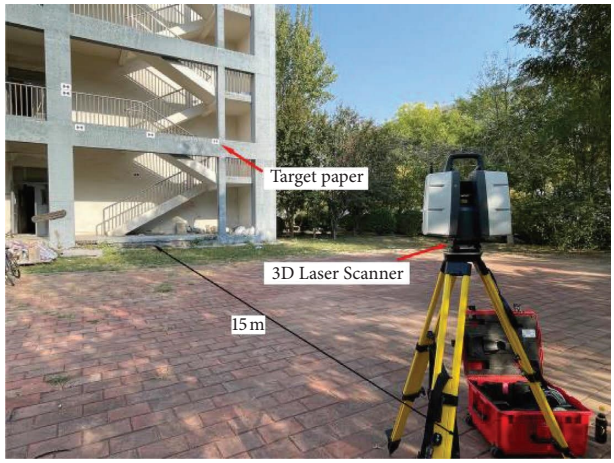

Figure 10: Configuration of validation tests.

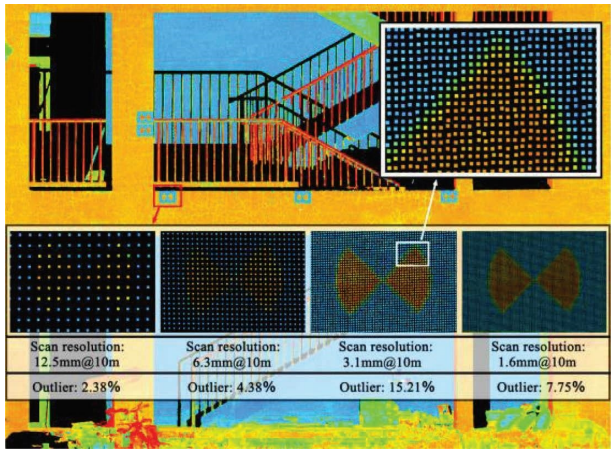

Figure 11: Scanning point cloud of verification experiment.

same extraction accuracy with a change in point cloud density. It is not affected by the scanning resolution and can obtain high-precision target center coordinates in the low-resolution point cloud data, which significantly shortens the data acquisition time in engineering applications, and the method is robust and feasible.

4.3.3. Algorithm Evaluation. The registration accuracy of the color-based iterative nearest point (colored ICP) directly determines the accuracy of the target center coordinate extraction, where the root mean square error (RMSE) is used as the registered error, and the formula is as follows:

$$\mathrm{RMSE} = \sqrt{\frac{1}{N_p}\sum_{i=1}^{N_p}\left\|\mathrm{Rp}_i + t - q_j\right\|^2}. \tag{15}$$

Figure 13 shows the trends of RMSE with the number of iterations for the four resolutions of the point cloud data. On the whole, the iterative convergence and matching accuracy of the algorithm are basically the same for different resolutions of the point cloud, and the RMSE of the algorithm tends to be stable when the number of iterations >5. Compared with the other resolution data, the low-density point cloud with the resolution of 12.5 m@10 m, due to the large difference in the number of point sets between the source and target point clouds, shows relatively more fluctuation after RMSE stabilizes, resulting in the change of matching in each iteration not as smooth as that of the high-density point cloud. However, the overall matching accuracy is controlled below 0.0012 m.

Figure 14 depicts the mean values of extraction accuracy and their standard errors for different extraction methods at four resolutions, and the error bars in the figure are described using standard errors. The average error accuracy of the conventional method increases with increasing scanning resolution because it can only extract the 3D coordinates of existing points in the point cloud. As the scanning resolution increases, the point cloud data near the center of the target become more intensive, and then, the extraction accuracy of the conventional method is improved. As can be seen from Figure 14, the proposed algorithm has the largest error at a scanning resolution of 3.1 mm@10 m. This can be explained by the variability of beam reflections, i.e., the distortion of intensity values in regions characterized by color transitions [55]. As shown in Figure 11, the intensity values of the point cloud are abnormal at the transition between the black and white colors of the target. The resolution of 3.1 mm@10 m has the highest percentage of outliers to the inner points in the target, amounting to 15.21%. The outliers at the edges of the sector region interfere with the registration accuracy of the colored ICP. This is because the principle of the method is to find the nearest point pair in two point clouds based on the intensity parameter [56]. The extraction accuracy of the algorithm remains below 1.3 mm for four resolutions, with slight fluctuations in accuracy. The standard error remains around 0.28 for all four resolutions, and the difference between the sample mean and the population mean is small, which is strongly representative of the sample data and a low extraction error for different qualities of the point cloud.

5. Project Example Analysis

This study focuses on the bearing replacement project for Jiuwangzhuang Bridge in Tianjin. The displacement of each girder was monitored during the bearing jacking operation using two methods: displacement sensors and a terrestrial 3D laser scanner combined with target papers.

5.1. 3D Laser Scanning Measurement Preparation. The target papers were posted at the diaphragm and the cover beam near each main girder to improve measurement quality and facilitate the pasting. In the following data processing, three methods were used: (1) the algorithm of this paper; (2) cyclone commercial software for processing point clouds, which employs the center of the target at the cap beam as the matching point for registration, both before and after jacking. Additionally, commercial software is employed to obtain the displacement difference value; (3) displacement

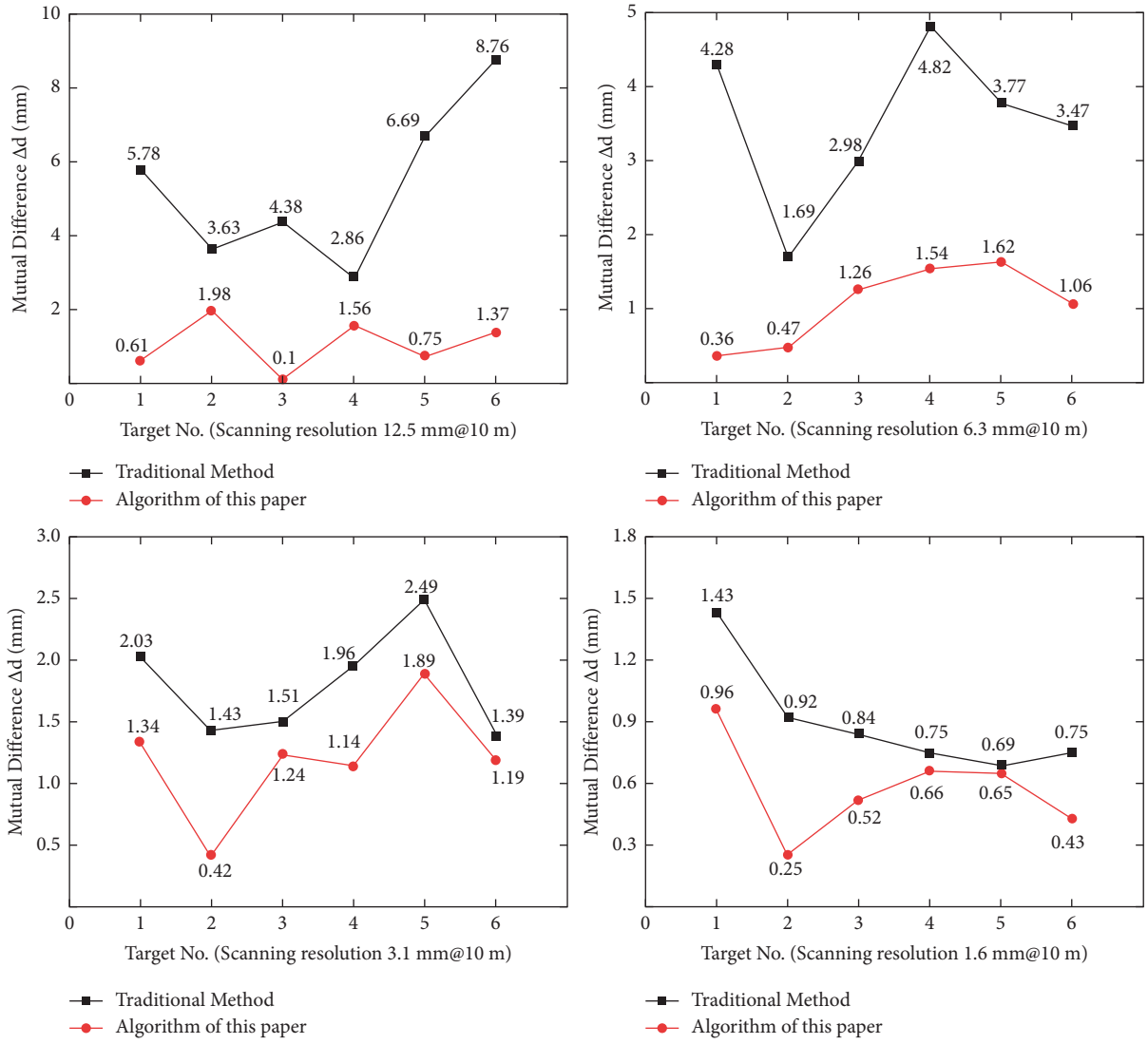

Figure 12: Multiresolution target center coordinates extraction error analysis chart.

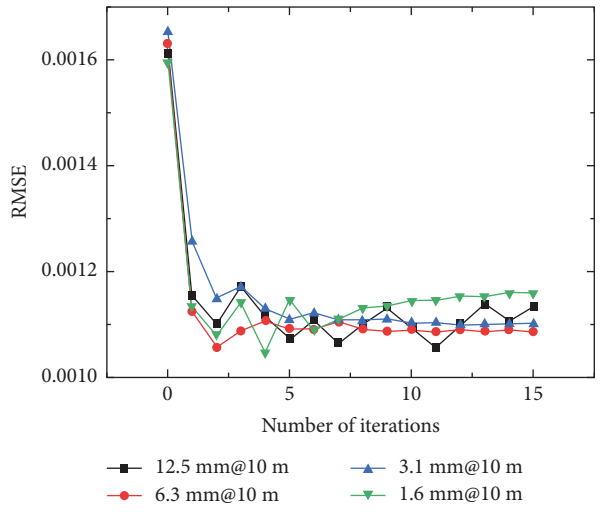

Figure 13: RMSE analysis for different iterations.

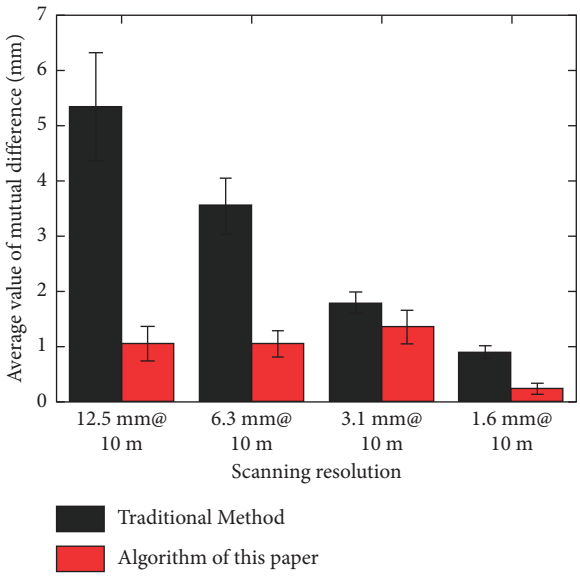

Figure 14: Standard error analysis of multiresolution data.

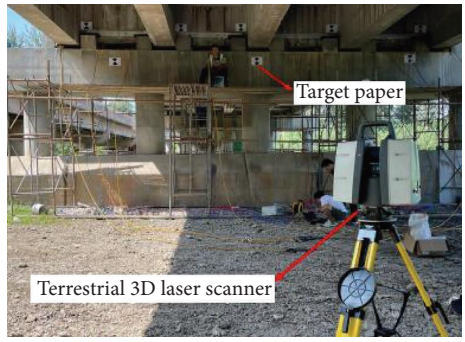

Figure 15: Scanning site for bearing replacement.

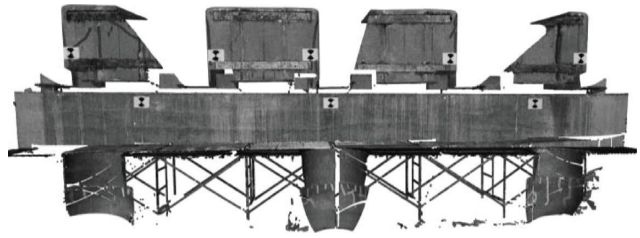

Figure 16: Scanning point cloud of the construction site.

sensors, which were deployed on-site as shown in Figure 15. The CPU used in the project example is Intel Core i7-7700HQ.

5.2. Target Point Cloud Preprocessing. Figure 16 displays the point cloud obtained during the jacked construction phase of the main girder. The initial number of point clouds acquired from the scanning process is 32,314,359. First, the point clouds with large intensity differences from the target are eliminated to achieve preliminary filtering. However, there are still a large number of outliers in the point cloud, which are removed using the radius-based point cloud filtering method, as shown in Figure 17. The number of filtered point clouds is 33,646.

As can be seen in Figure 17, with the point clouds bearing large differences from the intensity values of the target eliminated, there are still many discrete point clouds in space. According to the distribution features of the point clouds at the target, the point clouds with higher density are segmented using the clustering algorithm. To determine appropriate parameters eps and min_points, different parameters are used to cluster the targets. The process for debugging the clustering parameters is shown in Figure 18.

As can be seen in Figure 18, with min_points fixed, the number of core points in each class increases with the increasing of eps. This is due to the fact that increasing eps causes the search neighborhood of each data point to become larger, and the point clouds closer to the target are included in the same class (red dashed line in Figure 18). When eps is fixed, the increase of min_points retains the real point cloud with less density from being successfully clustered (red dashed line in Figure 18). This is because as min_points increases, the number of data points within the eps neighborhood required to be determined as core points increase, resulting in only the higher density point clouds clustered into one class. To ensure the rate and effect of clustering, 0.15 and 400 are chosen as the values of eps and min_points, respectively, for the extraction of clusters of target point clouds, and the clustering results are shown in Figure 19.

The point clouds of different colors in Figure 19 represent different classes. The DBSCAN clustering algorithm has successfully segmented and distinguished the targets. However, the algorithm also classifies other high-density point clouds in the point cloud into a class. By calculating the bounding box of each class of point clouds to determine its size, the point clouds with large differences from the target size are eliminated. Finally, all the targets are successfully extracted, as shown in Figure 20.

5.3. Planar Target Center Coordinate Extraction. The standard point cloud model of the target paper is shown in Figure 21(a). The normal vectors of the source and target point clouds are calculated before matching, which can greatly reduce the root mean square error in the initial matching and provide a better initial position for the two point clouds to be matched. The initial matching result of the target after one iteration of the algorithm is shown in Figure 21(b), which shows that the initial positions of the two point cloud planes have a larger overlap after one iteration of the algorithm.

In this paper, two conditions were set to terminate the iterative matching—the point cloud overlap area (fitness) and the root mean square error (RMSE). The final matching results are shown in Figure 21(c), where the red area is the overlap between the source point cloud (standard point cloud model) and the target point cloud, and it can be seen

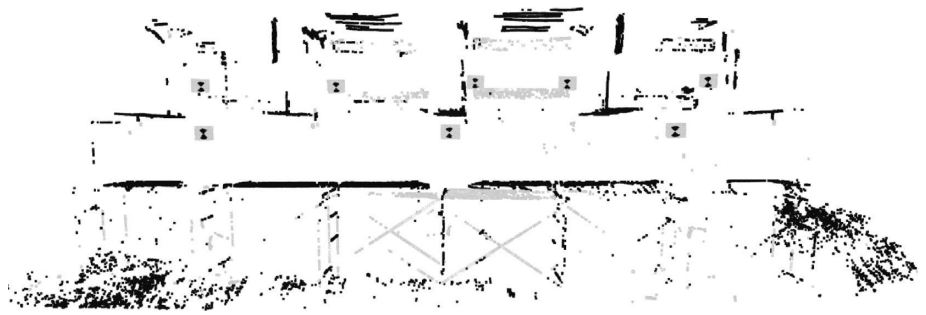

Figure 17: Filtered point cloud data based on target intensity values.

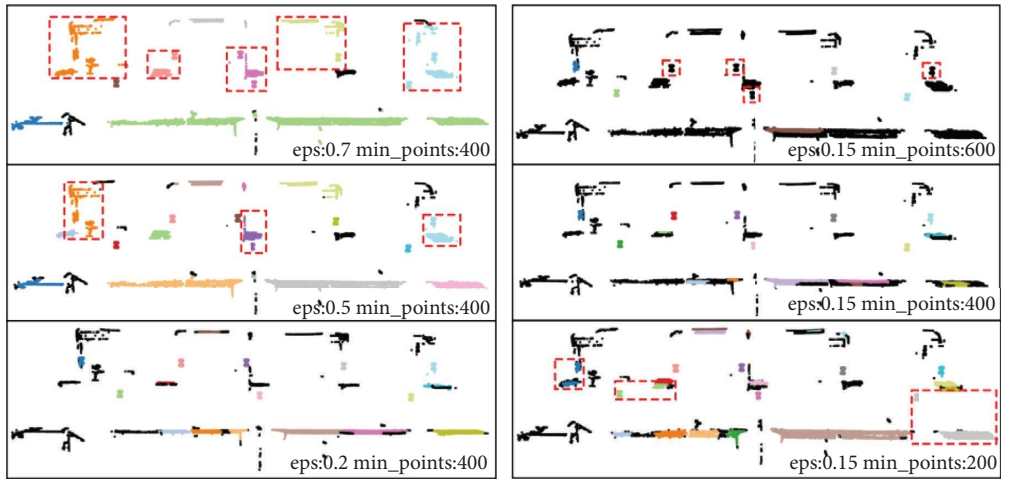

Figure 18: DBSCAN parameter debugging effect diagram.

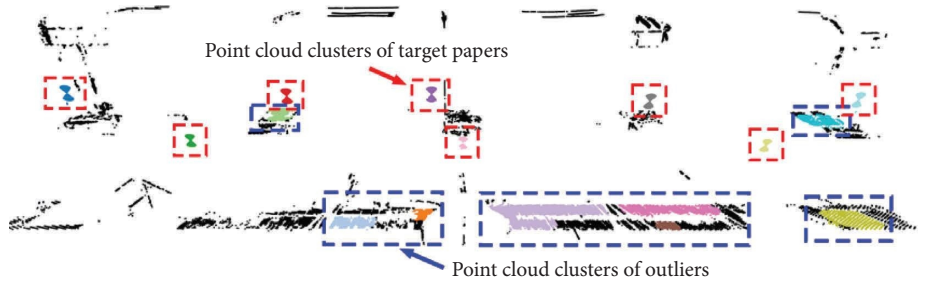

Figure 19: Point cloud data after DBSCAN clustering.

that the black sector of the two targets completely overlaps and the RMSE of the point cloud matching is stable at 0.00115 m. The matching results of all target papers after the jacking is completed are shown in Figure 22.

To facilitate subsequent applications, the recommended values of some parameters and the time spent to fine-tune them are listed in Table 1. Most parameters are insensitive to values within the recommended range. Thus, subsequent applications can fine-tune the parameters in a brief time. Therefore, the proposed method can save time compared to existing practices despite considering the fine-tuning procedure.

5.4. Girder Jacking Displacement Monitoring. Figures 23 and 24 depict the three calculated results of the displacement difference of each piece of the girder during jacking and dropping, respectively.

In this paper, the data acquired by displacement sensors are used as the theoretical standard to analyze three kinds of girder jacking displacements obtained through point cloud data. From Figures 23 and 24, it can be seen that the elevation difference values calculated using cyclone software are generally close to the theoretical values, but the data accuracy fluctuates more and the scanning time is longer compared with the algorithm in this paper. The elevation

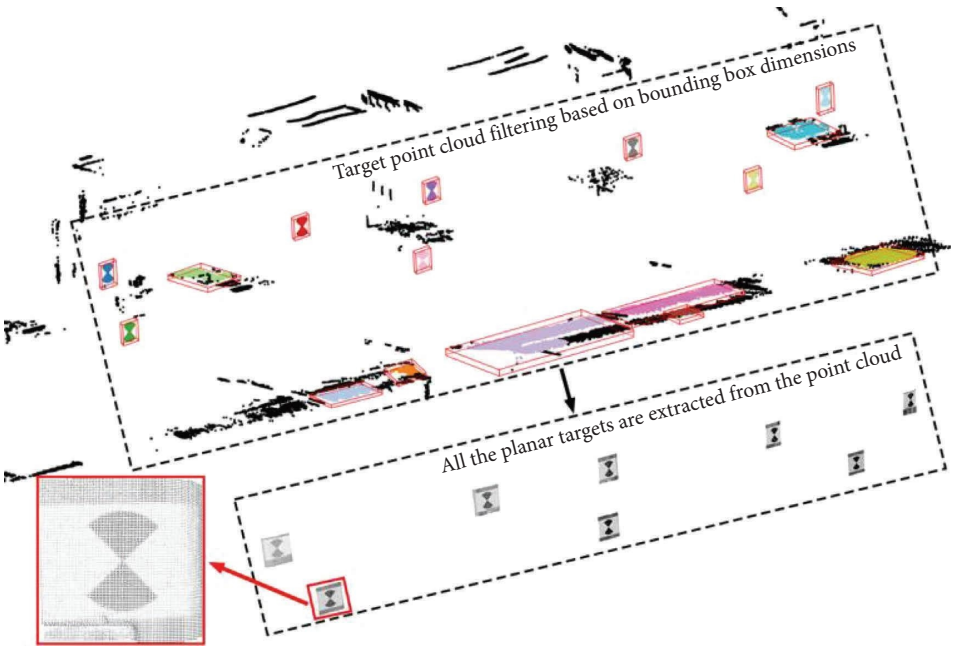

Figure 20: Filtering target paper point clouds using bounding box dimensions.

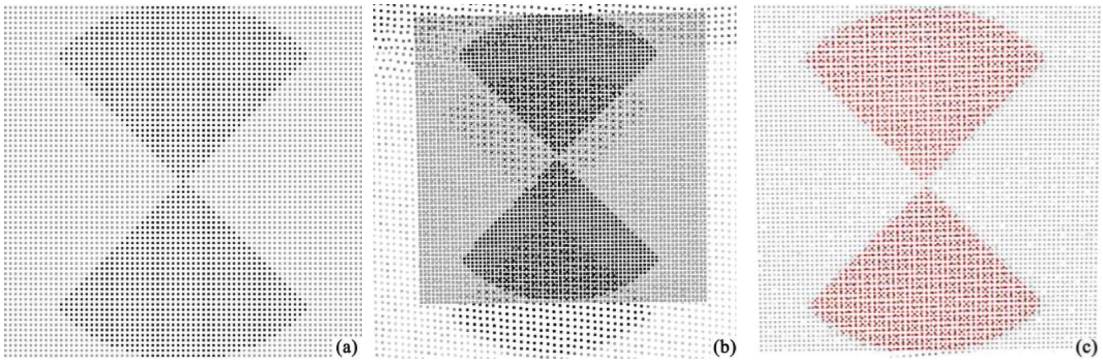

Figure 21: Process of matching target using colored ICP: (a) standard point cloud model of target paper, (b) the result of the proposed algorithm's first matching, and (c) the final result of algorithm matching.

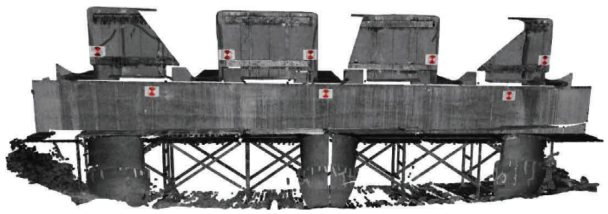

Figure 22: Final matching results for all targets.

difference calculated by the algorithm in this paper is the closest to the theoretical value, and the deviation is basically within 1 mm. Also, owing to the iterative matching algorithm in this paper, the target center calculation accuracy reaches submillimeters, which is the same as the displacement sensor. The above analysis shows that the algorithm proposed in this paper has the highest accuracy of target center extraction and the lowest operational complexity.

The comparison of the time required for the proposed method with commercial software to locate the target and the use of displacement sensors is listed in Table 2. The time consumed by the proposed method includes the acquisition time t_1 for the base point cloud data, the time t_2 for executing the algorithm to identify the targets and perform displacement calculations, and the time t_3 for the setup and debugging of the equipment. The application of point cloud commercial software for the computation of the main girder jacking displacement requires extracting target papers by employing the built-in planar target recognition function of TLS. Therefore, the method increases the consumed time t_4 to manually roughly locate the targets using TLS and the time t_5 for TLS to perform high-accuracy scanning in the vicinity of the approximated position. The amount of time required for utilizing the displacement sensor is solely t_3. T represents the total time required for each approach. The variables t_1, t_2, and t_5 represent the time during which the

Table 1: Time spent to fine-tune parameters and recommended values.

Parameters		Recommended values	Time for the first application (min)	Time for subsequent applications (min)
Coarse extraction of target PCD	Intensity filtering	int: I_{min} to 0.078 and 0.78 to I_{max}	5	1
	Outlier removal	nbPts: 50 ε-radius: 1.2 d_{pt} to 1.5 d_{pt}	8	2
	DBSCAN	minPts: 400 eps: 0.1 to 1.1 d_{sd}	11	2
	Bounding box filtering	d_x: 0.05 to 0.2 d_y: 0 to 0.1 d_z: 0.1 to 0.3	1	1
Extraction of target center coordinates	KNN	knn: 200	2	1
	Normal estimation	ε-radius: 0.8 d_{pd} to 1.2 d_{pd} max Pts: 30	6	1
	Colored ICP	rmse: 10^{-6} max Iter: 50	5	0.5

I_{min}: lowest intensity value in the point cloud, I_{max}: highest intensity value in the point cloud, d_{pt}: width of target paper, d_{sd}: diameter of the quarter-circle in the target paper, d_x: length of the bounding box along the x direction, d_y: length of the bounding box along the y direction, d_z: length of the bounding box along the z direction, and d_{pd}: average distance between two neighboring points.

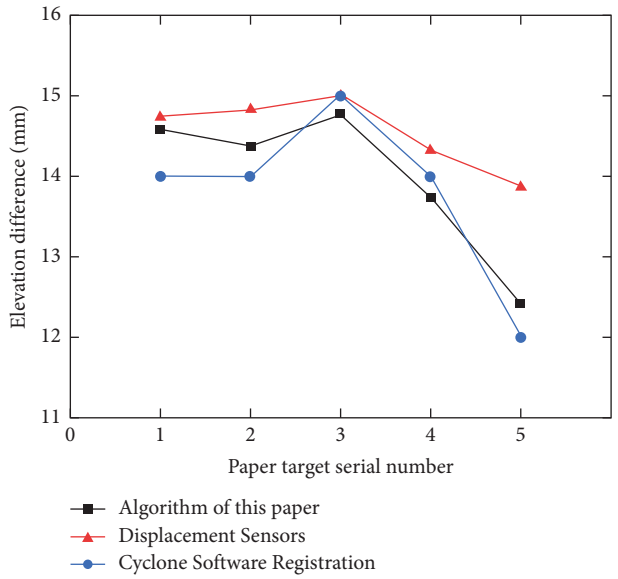

Figure 23: Girder jacking displacement.

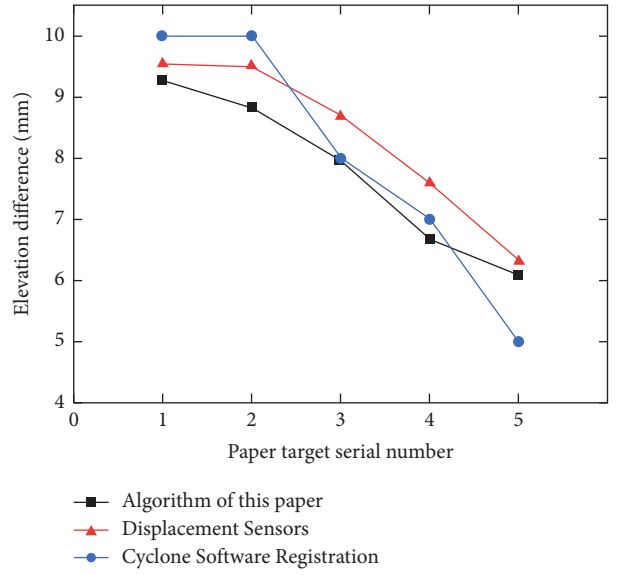

Figure 24: Girder drop displacement.

Table 2: Time required for the three monitoring methods.

	t_1 (s)	t_2 (s)	t_3 (s)	t_4 (s)	t_5 (s)	T (s)
Proposed method	12.0	3.6	138.0	—	—	153.6
Commercial software	79.0	7.5	138.0	307.0	208.0	739.5
Displacement sensor	—	—	1793.0	—	—	1793.0

equipment and algorithms operate, independent of any influence from human subjectivity. t_3 is the time for two skilled workers to perform the operation, and the time required can be further reduced if there are more workers. t_4 does not vary with the number of workers. Based on operational experience, this value varies slightly depending on the proficiency of the workers.

As can be seen from Table 2, the proposed method exhibits the shortest overall duration, with about 90% of the total time being allocated to the equipment setup phase. The proposed method demonstrates a significant time-saving of 98% during the data acquisition phase and a substantial reduction in monitoring duration compared to conventional commercial software approaches for target extraction. The

total time spent using the displacement sensor is the longest, which is 11.7 times longer than the proposed method. In addition, the main girder of the project is comprised of five T-shaped girders. Therefore, the time required for the aforementioned statistics is determined by measuring the displacement of five monitoring sites. The time required to use both commercial software and displacement sensors increases significantly with the number of monitoring sites. The proposed method exhibits a time requirement that is mostly unaffected by the number of monitoring sites and merely necessitates a greater consumption of target paper. Thus, the approach employed in this research does not impede the process of bearing replacement and exhibits better efficacy.

6. Conclusion

In this paper, a fully automated method for rapid acquisition of target paper displacement using 3D laser scanning is proposed after its successful application in monitoring the transverse synchronization of the jacking displacement of the main girder of an assembled multigirder bridge, with the following main conclusions:

(1) The strategy of using a 3D laser scanner combined with target papers for monitoring the transverse displacement of assembled multigirder jacking can significantly reduce the operational difficulty in displacement monitoring.

(2) Based on the intensity information of the point cloud, the DBSCAN clustering and bounding box algorithm, and point cloud processing technology, the intelligent extraction of planar targets in the point cloud can be realized.

(3) By creating a standard point cloud model of a planar target and using the colored ICP algorithm, the center coordinates of a planar target can be extracted quickly from the point cloud.

(4) The proposed algorithm can extract the target center coordinates in the low-resolution point cloud with high accuracy, and the acquisition time of the PCD can be reduced by 98% compared with the traditional method. The accuracy of the target center extraction is retained below 1.3 mm with a small accuracy fluctuation range in both experiments and applications. Its excellent iterative convergence of the matching process, low error, and small standard error of the sampled data can fully meet the application requirements.

The main contribution of the study is the development and validation of the automatic multiobjective displacement monitoring technique in main girder jacking. The application of point cloud attribute information and the ICP algorithm in feature point solving also provides a new approach for unstructured feature extraction from point clouds.

Nomenclature

P_T: Laser-transmitted power emitted by terrestrial laser scanners
P_R: Laser received power of terrestrial laser scanners
η_{Sys}: System transmission coefficient of the scanner
η_{Atm}: Atmospheric transport factor
α: Angle of incidence of the laser emitted by the scanner
R_s: Scanning range of laser scanners
ρ: Reflectance of the measured object
datamax: Upper limit of point cloud intensity for extracting valid points
datamin: Lower limit of point cloud intensity for extracting valid points
nb_points: Minimum number of points in the sphere for outlier removal algorithms
R_i: Radius of the sphere for outlier removal algorithms
eps: Radius of the circle in DBSCAN
min_points: Threshold for the number of points within a circle in DBSCAN
Datasize: Range of standard point cloud model generation
ρ_s: Point cloud density for standard point cloud model
θ_s: Radian values for standard point cloud models
R: Radius parameters for standard point cloud models
n: Normal vector of the point cloud plane
Δd: Mutual difference between theoretical and matched values
I_{min}: Lowest intensity value in the point cloud
I_{max}: Highest intensity value in the point cloud
d_{pt}: Width of the target paper
d_{sd}: Diameter of the quarter-circle in the target paper
d_x: Length of the bounding box along the x direction
d_y: Length of the bounding box along the y direction
d_z: Length of the bounding box along the z direction
d_{pd}: Average distance between two neighboring points
RMSE: Root mean square error
fitness: Overlapping areas of point clouds in fine matching.

Data Availability

The data used to support the findings of this study are available from the corresponding author upon request.

Disclosure

The opinions expressed in this paper belong solely to the authors.

Conflicts of Interest

The authors declare that they have no conflicts of interest.

Acknowledgments

The authors greatly appreciate the financial support provided by the National Natural Science Foundation of China (51978236) and the Tianjin Transportation Science and Technology Development Plan Project (2023-50).

References

[1] F. Ma, H. Wang, X. Cheng, D. Feng, G. Wu, and S. Hou, "Experimental investigation and application evaluation case of an adjustable height temporary support for bearing replacement in large-tonnage HSR bridges," *Journal of Bridge Engineering*, vol. 27, no. 5, 2022.

[2] F. Ma, H. Li, S. Hou, X. Kang, and G. Wu, "Defect investigation and replacement implementation of bearings for long-span continuous box girder bridges under operating high-speed railway networks: a case study," *Structure and Infrastructure Engineering*, vol. 18, no. 5, pp. 678–693, 2022.

[3] F. Ma, X. Cheng, X. Zhu et al., "Safety monitoring of bearing replacement for a concrete high-speed railway bridge based on acoustic emission," *Journal of Performance of Constructed Facilities*, vol. 36, no. 3, pp. 1–10, 2022.

[4] F. Li, P. Wu, and X. Yan, "Analysis and monitoring on jacking construction of continuous box girder bridge," *Computers and Concrete*, vol. 16, no. 1, pp. 49–65, 2015.

[5] F. Schill, C. Michel, and A. Firus, "Contactless deformation monitoring of bridges with spatio-temporal resolution: profile scanning and microwave interferometry," *Sensors*, vol. 22, no. 23, p. 9562, 2022.

[6] X. Li, E. Deng, Y. Wang, and Y. Ni, "3D laser scanning for predicting the alignment of large-span segmental precast assembled concrete cable-stayed bridges," *Automation in Construction*, vol. 155, 2023.

[7] Y. Li, B. Wu, and X. Ge, "Structural segmentation and classification of mobile laser scanning point clouds with large variations in point density," *ISPRS Journal of Photogrammetry and Remote Sensing*, vol. 153, no. 0, pp. 151–165, 2019.

[8] Q. Wu, J. Liu, C. Gao, B. Wang, G. Shen, and Z. Li, "Improved RANSAC point cloud spherical target detection and parameter estimation method based on principal curvature constraint," *Sensors*, vol. 22, no. 15, p. 5850, 2022.

[9] W. Liu, "Novel method for sphere target detection and center estimation from mobile terrestrial laser scanner data," *Measurement*, vol. 137, no. 0, pp. 617–623, 2019.

[10] Y. Shi, G. Zhao, C. Hu, M. Wang, M. Shi, and H. Ma, "Comparative study of the representative algorithms for fitting spherical target based on point cloud," *IEEE Transactions on Geoscience and Remote Sensing*, vol. 60, no. 1, pp. 1–16, 2022.

[11] M. Camurri, R. Vezzani, and R. Cucchiara, "3D Hough transform for sphere recognition on point clouds," *Machine Vision and Applications*, vol. 25, no. 7, pp. 1877–1891, 2014.

[12] Y. Wang, H. Shi, Y. Zhang, and D. Zhang, "Automatic registration of laser point cloud using precisely located sphere targets," *Journal of Applied Remote Sensing*, vol. 8, no. 1, 2014.

[13] G. Cheng, J. Liu, N. Cui, H. Hu, C. Xu, and J. Tang, "Virtual trial assembly of large steel members with bolted connections based on point cloud data," *Automation in Construction*, vol. 151, 2023.

[14] B. V. Farahani, F. Barros, P. J. Sousa, P. J. Tavares, and P. M. G. P. Moreira, "A railway tunnel structural monitoring methodology proposal for predictive maintenance," *Structural Control and Health Monitoring*, vol. 27, no. 8, pp. 1–15, 2020.

[15] D. Liang, Z. Zhang, C. Sui, J. Pu, L. C. Su, and K. Zhao, "Performance assessment of self-anchored suspension footbridge using 3D laser scanning," *Structural Control and Health Monitoring*, vol. 29, no. 8, p. e2978, 2022.

[16] G. Cha, S.-H. Sim, S. Park, and T. Oh, "LiDAR-based bridge displacement estimation using 3D spatial optimization," *Sensors*, vol. 20, no. 24, p. 7117, 2020.

[17] J. Yunmei, W. Huifeng, C. Haoyi et al., "Multi-point detection method of dynamic deflection of super long-span bridge based on chain laser model," *Measurement*, vol. 209, 2023.

[18] V. Zvegintsev and V. Kislovsky, "Automatic linear monitoring method of rigid skeleton arch bridge based on point cloud," *Science Technology and Engineering*, vol. 22, no. 36, pp. 16211–16218, 2022.

[19] Y. Shi, G. Zhao, M. Wang, and Y. Xu, "An adaptive grid search algorithm for fitting spherical target of terrestrial LiDAR," *Measurement*, vol. 198, 2022.

[20] J. Li, D. Zheng, Q. Lan, and Q. Liu, "A spherical targets fitting method for terrestrial laser scanning data," *International Symposium on Lidar and Radar Mapping*, vol. 8286, 2011.

[21] P. Stałowska, C. Suchocki, and M. Rutkowska, "Crack detection in building walls based on geometric and radiometric point cloud information," *Automation in Construction*, vol. 134, 2022.

[22] X. Zhou, J. Liu, G. Cheng, D. Li, and Y. F. Chen, "Automated locating of replaceable coupling steel beam using terrestrial laser scanning," *Automation in Construction*, vol. 122, 2021.

[23] A. Habib and Y.-J. Lin, "Multi-class simultaneous adaptive segmentation and quality control of point cloud data," *Remote Sensing*, vol. 8, no. 2, p. 104, 2016.

[24] S. Yoshizawa, A. Belyaev, H. Yokota, and H.-P. Seidel, "Fast, robust, and faithful methods for detecting crest lines on meshes," *Computer Aided Geometric Design*, vol. 25, no. 8, pp. 545–560, 2008.

[25] M. A. F. R. M. Scaioni, *Investigations about the Accuracy of Target Measurement for Deformation Monitoring, Politecnico di Milano, DIIAR*, Polo Regionale di Lecco, Italy, 2008.

[26] Z. W. C. Brenner, "Point Based Registration of Terrestrial Laser Data Using Intensity and Geometry Features," in *Proceedings of the 21st ISPRS International Congress for Photogrammetry and Remote Sensing*, Changsha, China, May 2008.

[27] J. Liu, N. Cui, X. Zhou et al., "Intelligent inspection method of house dimensional quality based on 3D laser scanning," *Journal of Building Science and Engineering*, vol. 39, no. 4, pp. 71–80, 2022.

[28] Y. Alshawabkeh, "Linear feature extraction from point cloud using color information," *Heritage Science*, vol. 8, no. 1, p. 28, 2020.

[29] B. Colford, M. Chiarello, C. Hendy, J. Sandberg, F. Biondini, and D. Frangopol, "Bearing Replacement and Strengthening of Forth Road Bridge Approach Viaducts," *UK, Bridge Maintenance, Safety, Management, Resilience and Sustainability*, vol. 167, pp. 1282–1287, 2012.

[30] B. Colford, M. Chiarello, C. R. Hendy, H. Pouya, J. Sandberg, and P. Smout, "Bearing replacements for forth road bridge approach viaducts," *Proceedings of the Institution of Civil Engineers-Bridge Engineering*, vol. 167, no. 3, pp. 170–182, 2014.

[31] D. A. Smith and C. R. Hendy, "Strengthening of irwell valley bridge, UK," *Proceedings-Institution of Civil Engineers: Bridge Engineering*, vol. 161, no. 1, pp. 33–43, 2008.

[32] J. Park, Q.-Y. Zhou, and V. Koltun, "Colored point cloud registration revisited," *Proceedings of the IEEE International Conference on Computer Vision*, pp. 143–152, 2017.

[33] M. Ester, H.-P. Kriegel, and J. Sander, "A Density-Based Algorithm for Discovering Clusters in Large Spatial Databases with Noise," in *Proceedings of the Second International Conference on Knowledge Discovery and Data Mining*, Portland Oregon, August 1999.

[34] C. Suchocki, M. Damiecka-Suchocka, J. Katzer, J. Janicka, J. Rapinski, and P. Stalowska, "Remote detection of moisture and bio-deterioration of building walls by time-of-flight and phase-shift terrestrial laser scanners," *Remote Sensing*, vol. 12, no. 11, p. 1708, 2020.

[35] S. P. Levashev, "Segmentation of a point cloud by data on laser scanning intensities," *Pattern Recognition and Image Analysis*, vol. 29, no. 1, pp. 144–155, 2019.

[36] T. Xu, L. Xu, B. Yang, X. Li, and J. Yao, "Terrestrial laser scanning intensity correction by piecewise fitting and overlap-driven adjustment," *Remote Sensing*, vol. 9, no. 11, p. 1090, 2017.

[37] K. Tan and X. Cheng, "Correction of incidence angle and distance effects on TLS intensity data based on reference targets," *Remote Sensing*, vol. 8, no. 3, p. 251, 2016.

[38] T. Xu, L. Xu, X. Li, and J. Yao, "Detection of water leakage in underground tunnels using corrected intensity data and 3D point cloud of terrestrial laser scanning," *IEEE Access*, vol. 6, pp. 32471–32480, 2018.

[39] M. Balaguer-Puig, A. Molada-Tebar, A. Marques-Mateu, and J. L. Lerma, "Characterization of intensity values on terrestrial laser scanning for recording enhancement," *SPRS International Scientific Committee on Heritage Documentation (CIPA) 26th International CIPA Symposium-Digital Workflows for Heritage Conservation*, vol. 42, pp. 49–55, 2017.

[40] Z. Shen, P. Tang, O. Kanaan, and Y. K. Cho, *As-Built Error Modeling for Effective 3D Laser Scanning on Construction Sites*, ASCE Library, Reston, VA, USA, 2013.

[41] A. Julin, M. Kurkela, T. Rantanen et al., "Evaluating the quality of TLS point cloud colorization," *Remote Sensing*, vol. 12, no. 17, p. 2748, 2020.

[42] T. O. Chan, H. Xiao, L. Liu et al., "A post-scan point cloud colorization method for cultural heritage documentation," *ISPRS International Journal of Geo-Information*, vol. 10, no. 11, p. 737, 2021.

[43] G. Kavulya, F. Jazizadeh, and B. Becerik-Gerber, *Effects of Color, Distance, and Incident Angle on Quality of 3D Point Clouds*, ASCE Library, Reston, VA, USA, 2011.

[44] R. Qi and W. Liang, "Research on the integrated manipulator of point cloud measurement and precise cutting for waste nuclear tank," *Industrial Robot: The International Journal of Robotics Research and Application*, vol. 49, no. 4, pp. 696–707, 2022.

[45] Y. Xu, Z. Ye, R. Huang, L. Hoegner, and U. Stilla, "Robust segmentation and localization of structural planes from photogrammetric point clouds in construction sites," *Automation in Construction*, vol. 117, 2020.

[46] M. Huang, X. Y. Wu, X. L. Liu, T. H. Meng, and P. Y. Zhu, "Integration of constructive solid geometry and boundary representation (CSG-BRep) for 3D modeling of underground cable wells from point clouds," *Remote Sensing*, vol. 12, no. 9, p. 1452, 2020.

[47] C. R. Harris, K. J. Millman, S. J. van der Walt et al., "Array programming with NumPy," *Nature*, vol. 585, no. 7825, pp. 357–362, 2020.

[48] L. Li, X. Cao, and J. Sun, "Three-dimensional point cloud registration based on normal vector angle," *Journal of The Indian Society of Remote Sensing*, vol. 47, no. 4, pp. 585–593, 2019.

[49] J. Wang, B. Wu, and J. Kang, "Registration of 3D point clouds using a local descriptor based on grid point normal," *Applied Optics*, vol. 60, no. 28, pp. 8818–8828, 2021.

[50] X. Zhan, Y. Cai, H. Li, Y. Li, and P. He, "A point cloud registration algorithm based on normal vector and particle swarm optimization," *Measurement and Control (United Kingdom)*, vol. 53, no. 3-4, pp. 265–275, 2019.

[51] A. Wu, Y. Ding, J. Mao, and X. Zhang, "A fast point clouds registration algorithm based on ISS-USC feature for the 3D laser scanner," *Algorithms*, vol. 15, no. 10, p. 389, 2022.

[52] W. Yuan, D. Choi, and D. Bolkas, "GNSS-IMU-assisted colored ICP for UAV-LiDAR point cloud registration of peach trees," *Computers and Electronics in Agriculture*, vol. 197, 2022.

[53] C. Hajiyev, "Generalized Rayleigh quotient based innovation covariance testing applied to sensor/actuator fault detection," *Measurement*, vol. 47, no. 1, pp. 804–812, 2014.

[54] T. Cover and P. Hart, "Nearest neighbor pattern classification," *IEEE Transactions on Information Theory*, vol. 13, no. 1, pp. 21–27, 1967.

[55] A. Fryskowska, "An improvement in the identification of the centres of checkerboard targets in point clouds using terrestrial laser scanning," *Sensors*, vol. 19, no. 4, p. 938, 2019.

[56] Y. Zhou, D. Han, K. Hu et al., "Accurate virtual trial assembly method of prefabricated steel components using terrestrial laser scanning," *Advances in Civil Engineering*, vol. 2021, Article ID 9916859, 15 pages, 2021.